Journal of Southeast University (English Edition) Vol. 39, No. 4, pp. 361 - 371 Dec. 2023 ISSN 1003—7985

Progressive collapse analysis of steel frames under fire based on high-temperature component model

Ding Runmin Fan Shenggang

(Key Laboratory of Concrete and Prestressed Concrete Structures of Ministry of Education, Southeast University, Nanjing 211189, China)
(School of Civil Engineering, Southeast University, Nanjing 211189, China)

Abstract: To explore the overall behavior response and progressive collapse mechanism of steel frame structures under fire, a progressive collapse test was conducted on a 1∶2 scale steel frame structure with a corner room subjected to fire. Consequently, the air temperature-time, component temperature-time, and frame displacement-time curves of the entire fire development process, as well as the progressive collapse failure mode of steel frame structures under fire, were obtained. A high-temperature component model of welded flange-bolted web connections was established using the component method, and a bilinear mathematical model for the moment-rotation angle curves of welded flange-bolted web connections at high temperatures was derived. On this basis, a finite element analysis model was established for the progressive collapse of steel frame structures under fire, including the high-temperature component model of welded flange-bolted web connections. The accuracy of the finite element analysis model was verified by comparison with the progressive collapse test results, and the progressive collapse mechanism of steel frame structures under fire was revealed. The results show that under fire within the corner room of a steel frame structure, even though the stress ratio of the corner column is the lowest, primarily due to its lower axial constraint than the inner and side columns, the corner column will first lose its load-bearing capacity and withdraw from work. This triggers the progressive collapse failure of the steel frame structure.

Key words: fire; component model; welded flange-bolted web connection; progressive collapse; steel frame
DOI: 10.3969/j.issn.1003-7985.2023.04.005

The connection performance of beam-to-column joints is a key factor in evaluating the overall stability and robustness of steel frame structures. Under normal service conditions, the beam-to-column joints mainly transfer bending moments and shear forces. However, if the load-bearing components are damaged, the force mechanism of beam-to-column joints will change to mainly transfer tensile force due to catenary action, which significantly impacts the redistribution of internal forces inside the remaining structure. Moreover, due to the degradation of material properties at elevated temperatures, the rotational stiffness of beam-to-column joints will significantly decrease as the temperature increases[1]. Therefore, mastering the behavior of beam-to-column joints at elevated temperatures is a key task in studying the progressive collapse resistance of steel frame structures under fire.

The welded flange-bolted web connection has been widely used as a steel moment connection, and many experimental and theoretical studies have been conducted on its performance at room temperature. For instance, Shi et al.[2] conducted low cyclic loading tests on eight welded flange-bolted web connection joints. They demonstrated the impact of the shape and size of the weld access hole on the failure mode and hysteretic performance of joints. Lew et al.[3] conducted progressive collapse tests on two full-scale steel beam-column assemblies to investigate the failure modes and rotational capacities of two different welded flange-bolted web connection types under a column removal scenario. Wang et al.[4] conducted a vertical load test on the substructure of a beam-to-column welded flange-bolted web connection. They found that the moment-rotation angle (M-θ) curves of welded flange-bolted web connections can be divided into two stages and represented by double lines. Ma[5] proposed a new spring model defined by the characteristic points of M-θ curves to simulate the rotation of beam-to-column welded flange-bolted web connections in steel frames.

With the increasing attention paid to the safety of steel structures under fire, there is a growing number of research on the fire resistance of welded flange-bolted web connections. For instance, Wang and Dong[6] conducted an experimental study on the behavior of welded flange-bolted web connections under fire. They found that the welding seam is the weakness of the fire resistance of the connections, and the buckling of the column flange at the joint region will cause a significant joint rotation under fire. Mao et al.[7] investigated the variation law of the

Received 2023-06-12, **Revised** 2023-09-19.

Biographies: Ding Runmin (1995—), male, Ph. D. candidate; Fan Shenggang (corresponding author), male, doctor, professor, 101010393@seu.edu.cn.

Foundation items: The National Natural Science Foundation of China (No. 52278153, 51878146), Scientific Research Foundation of Graduate School of Southeast University.

Citation: Ding Runmin, Fan Shenggang. Progressive collapse analysis of steel frames under fire based on high-temperature component model[J]. Journal of Southeast University (English Edition), 2023, 39(4): 361 - 371. DOI: 10.3969/j.issn.1003-7985.2023.04.005.

stiffness of steel moment connections at elevated temperatures using a numerical simulation method. They found that the applied moments have significant effects on the stiffness of steel moment connections. Hu[8] proposed an M-θ model with temperature parameters for welded flange-bolted web connections at elevated temperatures. Fan et al.[9-10] conducted fire tests on four beam-to-column welded flange-bolted web composite joints. They proposed the formulas for calculating the flexural bearing capacity and initial rotational stiffness of the composite joints at elevated temperatures. Qiang et al.[11] conducted full-scale tests on four high-strength steel welded flange-bolted web connections at room and elevated temperatures. They compared their test results with the prediction results of codes in China and aboard and provided design suggestions for high-strength steel welded flange-bolted web connections.

The component method has been widely used in the simulation analysis of structures and components. Over the years, it has experienced significant growth and development. Initially, it was primarily employed for static analysis at room temperature[12-15]. Then, its scope expanded to encompass the study of rotational stiffness, stability, and load-bearing capacity of joints at high temperatures[16-18]. Now it has been widely used to study dynamic responses and progressive collapse of structures[19-26]. This paper aims to decompose the welded flange-bolted web connections into multiple parts based on the component method and finally provide an M-θ curve model suitable for different temperatures and connection sizes. In this way, it is convenient for researchers and engineering designers to use the high-temperature M-θ curve model in the progressive collapse analysis of steel frames under fire.

To investigate the process and mechanism of progressive collapse of steel frame structures under fire, a progressive collapse test was conducted on a 1∶2 scale steel frame structure with a corner room subjected to fire. Then, a high-temperature component model was proposed for welded flange-bolted web connections, and its accuracy was verified using the existing fire tests of welded flange-bolted web composite joints[9-10]. The proposed high-temperature component model was applied to the progressive collapse analysis model of steel frame structures under fire. It was proved to be accurate by comparing with the progressive collapse test results. Finally, the progressive collapse mechanism of steel frame structures under fire was revealed.

1 Summary of the Progressive Collapse Test of Steel Frame under Fire

1.1 Test background

Currently, most research on the progressive collapse resistance of steel frame structures under fire adopts the numerical simulation method[27-29]. The finite element software, such as ABAQUS, Opensees, LS-DYNA, and VULCAN, have been widely used to simulate the progressive collapse process of steel frame structures under fire, analyze the causes of progressive collapse accidents, or improve the design method to resist progressive collapse[30-33]. The relevant experimental research is very scarce, and the research objects are all planar steel frame structures[34-35]. Due to the lack of consideration of real fire scenarios and the membrane effect of the floor, the existing progressive collapse tests cannot truly reflect the actual progressive collapse process of three-dimensional (3D) steel frame structures under fire. Therefore, it is necessary to carry out experimental research on the progressive collapse resistance of 3D steel frame structures under fire. The progressive collapse test was conducted on a 1∶2 scale two-story 2 × 2 span steel frame structure to control the cost and risk of the test and ensure the accuracy of the test.

1.2 Test setup

The plane size of the test frame was 6 m × 6 m, as shown in Fig. 1. The test frame had two floors (1.8 m for the first floor and 1.6 m for the second floor). The sectional sizes of the steel column, beam, and secondary beam of the test frame were selected as HW100 mm × 100 mm × 6 mm × 8 mm, HM150 mm × 100 mm × 6 mm × 9 mm, and HN150 mm × 75 mm × 5 mm × 7 mm, respectively. All steel components were made of Q235B. In the test frame, the column and beam were connected by the welded flange-bolted web connection (see Fig. 2), while the beam and secondary beam were connected by the hinged connection.

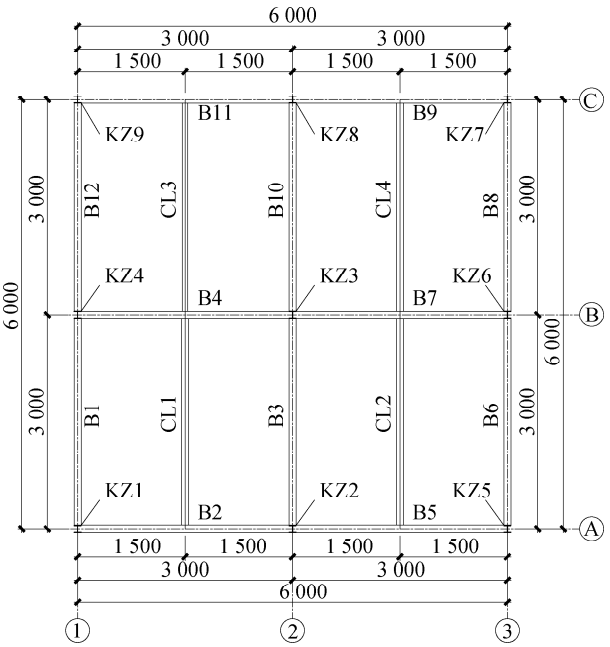

Fig. 1 Layout of the test frame (unit: mm)

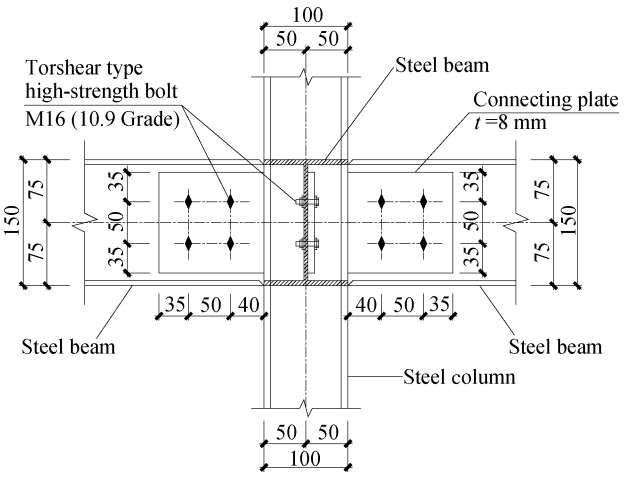

Fig. 2 Detailed construction of welded flange-bolted web connection (unit: mm)

The test frame adopted the cast-in-place concrete floor with a thickness of 80 mm and a concrete strength grade of C30. The strength grade of the reinforcement in the slab is HPB300, with a diameter and spacing of 8 and 150 mm, respectively. The column bases of the test frame are all open rigid column bases.

The four rooms on the first floor of the test frame were all wrapped with rock wool firewalls. One was stacked with four wooden piles ignited at the beginning of the test (regarded as Room A, the room where the fire occurred). The other three rooms each had a pan containing diesel fuel (see Fig. 3). The fire load density of Room A was selected as 1 455 MJ/m^2, which means a total of 1.6 m^3 of pine wood.

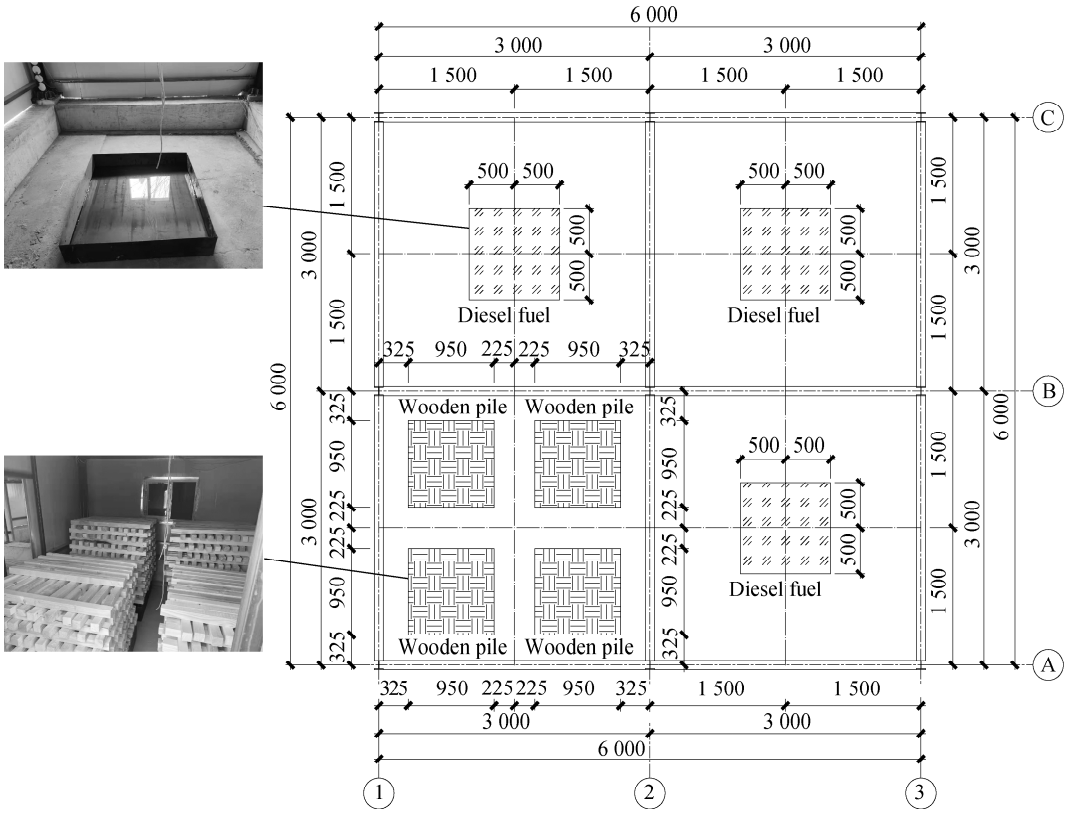

Fig. 3 Distribution of fire load (unit: mm)

In the test, the floor load was taken as 6.0 kPa to ensure that the stress ratio of the steel columns on the first floor of the frame reached 0.4. Hence, 44.24 t of sandbags were piled on the test frame. The fire resistance time of the fire-exposed components was controlled to 30 min to observe the progressive collapse of the test frame. Therefore, the steel columns and beams in Room A were coated with a certain thickness of fire-retardant paint (0.9 mm for steel columns and 0.6 mm for steel beams). Many K-type thermocouples were placed in the test frame to monitor the changes in the air and component temperatures. For a 3D steel frame structure, the direction of progressive collapse cannot be limited to a certain plane, meaning that the displacements of the test frame in three spatial directions (x, y, z) all need to be recorded in real time. Therefore, the noncontact digital image correction measurement method was adopted to monitor the entire progressive collapse process of the test frame under fire. Fig. 4 shows the overall view of the test frame.

1.3 Test results

The wooden piles in Room A underwent severe combustion after being ignited, and the air temperature of Room A rose rapidly. After ignition for 23 min 50 s, the

Fig. 4 Overall view of the test frame

test frame suddenly experienced a progressive collapse failure. The overall failure mode was the downward collapse of the corner room subjected to fire (see Fig. 5). The speed of the progressive collapse was extremely fast, and the entire failure progress did not exceed 1 s. However, this rapid progressive collapse process was recorded using high-speed cameras with a frame rate of 75 FPS. The captured images showed that the corner column in Room A was the first to completely destroy and withdraw from work. Almost at the same time, the surrounding steel columns completely lost their bearing capacity, resulting in the progressive collapse of the structure.

Fig. 5 Failure mode of the test frame

The air temperature in the rooms on the first floor of the test frame was monitored by the thermocouple tree hanging in the middle of each room. Fig. 6 shows the air temperature-time curves of Room A at different heights.

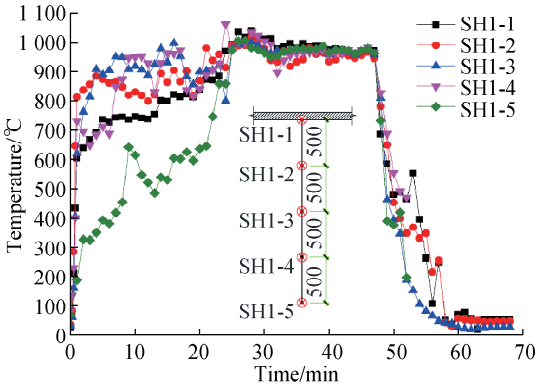

Fig. 6 Air temperature-time curves of Room A(unit: mm)

The component temperature-time curves of all steel members in Room A (steel columns KZ1-KZ4 and steel beams B1-B4) were also monitored in real time, as shown in Fig. 7.

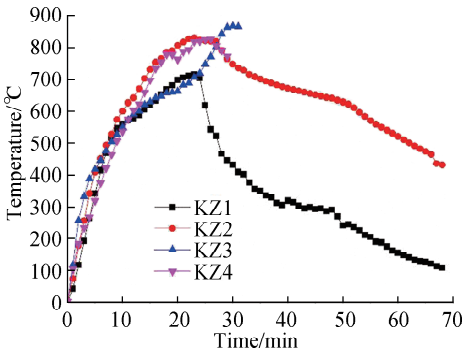

(a)

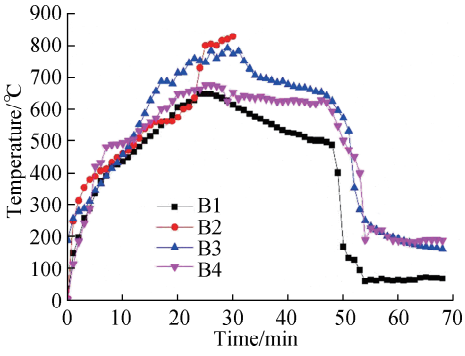

(b)

Fig. 7 Temperature-time curves of steel members in Room A. (a) Steel columns; (b) Steel beams

Figs. 6 and 7 show that the temperature field of compartment fire is evenly distributed. Moreover, to simplify the progressive collapse analysis of steel frame structures under fire, it can be assumed that all fire-exposed steel columns (or steam beams) in the room are subjected to the same fire action.

The white circular targets sprayed on the surface of steel members were tracked by six high-speed cameras. The spatial coordinates of these circular targets can be directly obtained as a function of time by processing the images taken using high-speed cameras. Due to space limitations, only the vertical displacement-time curves of steel columns KZ1 and KZ2 are given in Fig. 8. As shown in Fig. 8, the buckling failure of all steel columns in the steel frame occurred almost simultaneously due to the overall tie action provided by the beams and slabs.

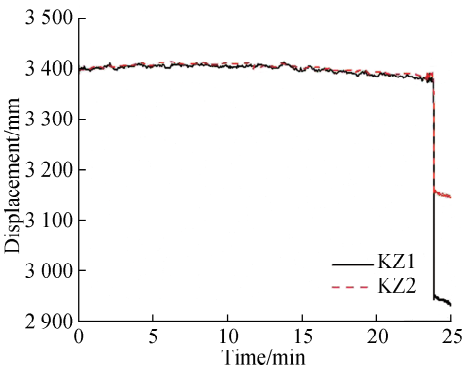

Fig. 8 Vertical displacement-time curves of steel columns

2 High-Temperature Component Model of Welded Flange-Bolted Web Connection

2.1 High-temperature component model

The basic principle of the component method is to decompose the connection into several basic components that only bear tensile, compressive, and rotational deformation according to their stress characteristics and then replace each basic component with a spring with the equivalent bearing capacity and stiffness. Finally, these springs are assembled for analysis[36]. In the component model of welded flange-bolted web connection, the deformation and force of the upper and lower flanges of the steel beam are equivalent to tensile or compressive springs, whereas the interaction between the web of steel beam and the connecting plate is equivalent to a rotational spring (see Fig. 9). To simplify the calculation, the shear deformation of the panel zone is ignored in the model, which is relatively small when the steel column has stiffeners at the joint region.

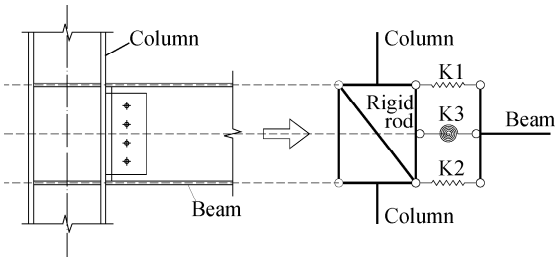

Fig. 9 Component model of welded flange-bolted web connection

Through several numerical simulation studies, Yim and Krauthammer[37] proposed a bilinear model to represent the M-θ curves of welded flange-bolted web connections at room temperature. The previous test results[3-4, 11] also indicated that using a bilinear model to represent the M-θ curves of welded flange-bolted web connections at room and elevated temperatures is reasonable. This is because the initial flexural stiffness of the welded flange-bolted web connection is mainly provided by the bending moment generated by the axial deformation of the upper and lower flanges of the steel beam, and the contribution of the web is very small at this period. However, after the flanges of the steel beam yield under tension and pressure, the flexural stiffness provided by the steel beam flanges rapidly decreases and becomes close to the flexural stiffness provided by the web. Therefore, the nonlinear springs K1 and K2 corresponding to the upper and lower flanges of the steel beam at temperature T can be assumed to be in the bilinear form (see Fig. 10(a)). The rotational spring K3 corresponding to the interaction between the web and connecting plate at temperature T can be considered linear (see Fig. 10(b)). The stiffness of K3 is much smaller than that of K1 and K2 in the elastic stage; however, it can no longer be ignored after the steel beam flanges enter plasticity, so simplifying the spring K3 as linear does not cause much error[4].

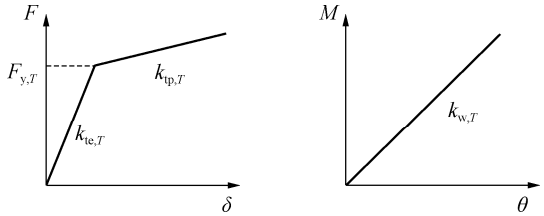

Fig. 10 Springs in the high-temperature component model. (a) K1 and K2; (b) K3

According to previous studies [4, 37], the elastic stiffness $k_{te,T}$ of K1 and K2 at temperature T can be calculated by

$$k_{te,T} = \frac{E_{bf,T} t_{bf} b_{bf}}{\rho_1 l_{co}} \tag{1}$$

The plastic stiffness $k_{tp,T}$ of K1 and K2 at temperature T is simply considered to have a proportional relationship with the elastic stiffness $k_{te,T}$, and it can be calculated by

$$k_{tp,T} = \frac{E'_{bf,T}}{E_{bf,T}} k_{te,T} \tag{2}$$

where $E_{bf,T}$ is the elastic modulus of steel materials at the steel beam flange and temperature T; t_{bf} and b_{bf} are the thickness and width of the steel beam flange, respectively; l_{co} is the length of the connecting plate; ρ_1 is an adjustment coefficient about effective length taken as 1.5[37]; $E'_{bf,T}$ is the tangent modulus of steel materials at the steel beam flange and temperature T, and $E'_{bf,T}/E_{bf,T}$ is usually taken as 0.01.

Assuming that the connecting plate undergoes uniform bending deformation, the rotational stiffness $k_{w,T}$ of K3 can be calculated by

$$k_{w,T} = \frac{E_{w,T} I_{co}}{\rho_2 l_{co}} \tag{3}$$

$$I_{co} = \frac{t_w h_{co}^3}{12} \tag{4}$$

where $E_{w,T}$ is the elastic modulus of steel materials at the web of steel beam and temperature T; t_w is the thickness of the web of steel beam; h_{co} is the height of the connecting plate; I_{co} is the cross-sectional moment of inertia of the connecting plate; ρ_2 is a coefficient related to joint structure, usually taken as 2.0.

Fig. 11 shows the bilinear model for the M-θ curve of welded flange-bolted web connection at temperature T, consisting of elastic deformation and plastic deformation stages. The gradient of the elastic deformation stage is donated by the elastic flexural stiffness $K_{e,T}$, whereas that of the plastic deformation stage is donated by the plastic flexural stiffness $K_{p,T}$. The bending moment correspond-

ing to the turning point is donated by the yield bending moment of connection $M_{y,T}$, and the rotation angle at this time is donated by the yield rotation angle of connection $\varphi_{y,T}$.

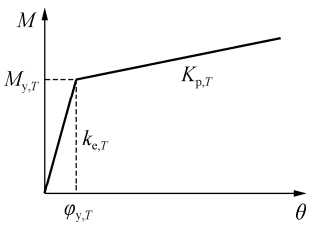

Fig. 11 Bilinear model for the M-θ curve of welded flange-bolted web connection

In the elastic deformation stage, it is assumed that the component model has a rotation angle of $\varphi_{e,T}$ at temperature T, as shown in Fig. 12. According to the displacement coordination and equilibrium equations, the following can be obtained:

$$M_{e,T} = (F_{K1,T} + F_{K2,T})\frac{h}{2} + M_{K3,T} \tag{5}$$

$$F_{K1,T} = F_{K2,T} = k_{te,T}\frac{h}{2}\varphi_{e,T} \tag{6}$$

$$M_{K3,T} = k_{w,T}\varphi_{e,T} \tag{7}$$

$$M_{e,T} = K_{e,T}\varphi_{e,T} \tag{8}$$

$$K_{e,T} = \frac{h^2}{2}k_{te,T} + k_{w,T} \tag{9}$$

where h is the height of the steel beam.

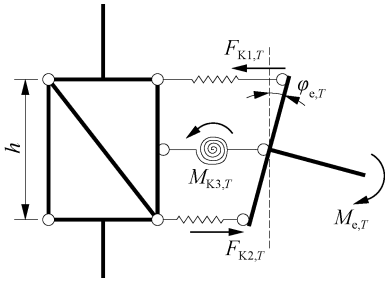

Fig. 12 Calculation diagram of internal forces of component model in the elastic deformation stage

Similarly, when the connection enters the plastic deformation stage and undergoes a plastic rotation angle of $\varphi_{p,T}$ at temperature T, the following can be obtained:

$$M_{p,T} = (F_{K1,T} + F_{K2,T})\frac{h}{2} + M_{K3,T} \tag{10}$$

$$F_{K1,T} = F_{K2,T} = F_{y,T} + k_{tp,T}\frac{h}{2}\varphi_{p,T} \tag{11}$$

$$M_{K3,T} = k_{w,T}(\varphi_{y,T} + \varphi_{p,T}) \tag{12}$$

$$M_{p,T} = K_{p,T}\varphi_{p,T} + M_{y,T} \tag{13}$$

$$M_{y,T} = F_{y,T}h + k_{w,T}\varphi_{y,T} \tag{14}$$

$$K_{p,T} = \frac{h^2}{2}k_{tp,T} + k_{w,T} \tag{15}$$

At the turning point of the M-θ curve at temperature T, through mechanical analysis, the following can be obtained:

$$F_{y,T} = f_{y,T}t_{bf}b_{bf} = k_{te,T}\frac{h}{2}\varphi_{y,T} \tag{16}$$

$$\varphi_{y,T} = \frac{2f_{y,T}t_{bf}b_{bf}}{k_{te,T}h} = \frac{2\rho_1 f_{y,T}l_{co}}{E_{bf,T}h} \tag{17}$$

$$M_{y,T} = K_{e,T}\varphi_{y,T} = \frac{2K_{e,T}f_{y,T}t_{bf}b_{bf}}{k_{te,T}h} \tag{18}$$

where $f_{y,T}$ is the yield strength of steel materials at temperature T.

2.2 Validation of component model

Based on the previous fire tests on three welded flange-bolted web composite joints[9-10], the traditional finite element software ABAQUS[38] was used to establish the member system models of beam-column substructures with the same geometric dimensions (see Fig. 13). After setting the mechanical performance parameters of each joint component through the spring element, the vertical displacement-time curve of each specimen obtained from the beam-column substructure model is compared with the test results (see Fig. 14). Fig. 14 shows that the finite element results for the deflection rate of beam end are significantly greater than the test results, except for specimen CJ-1, which was unable to maintain a stable load at

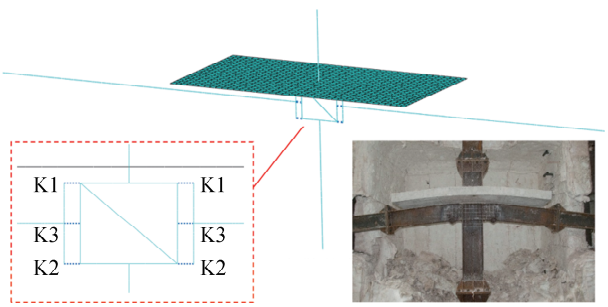

Fig. 13 Member system model of beam-column substructure

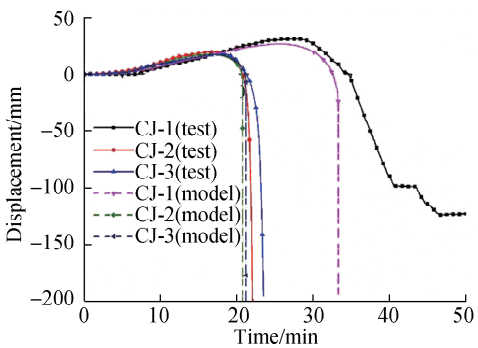

Fig. 14 Comparison of test results and model results

the end of the beam during the failure stage due to problems with the loading equipment. The finite element results for the vertical displacement-time curves of specimens CJ-2 and CJ-3 are consistent with the test results. The proposed high-temperature component model can accurately predict the stress state and mechanical properties of welded flange-bolted web connections in steel frame structures under fire.

3 Progressive Collapse Analysis Model of Steel Frames under Fire

3.1 Material constitutive models

In the progressive collapse analysis model, the constitutive model of steel materials adopted the stress-strain model of carbon steel at elevated temperatures provided by EC3[39]. Three tensile coupons were tested at room temperature, with a yield strength and elastic modulus of steel materials of 261.7 MPa and 199.725 GPa, respectively. The Poisson's ratio of steel materials was set to 0.30. The reduction coefficients of yield strength and elastic modulus of steel at high temperatures also adopted the high-temperature tensile test results, as presented in Table 1.

The temperature changes inside the concrete slab were monitored using pre-embedded thermocouples. The temperature monitoring results show that due to a large amount of water in the concrete slab, the temperatures inside the slab did not significantly increase during the progressive collapse process of the test frame and remained stable after reaching 100 ℃. Therefore, the internal temperature of the concrete slab remains at the ambient temperature, and the reduction of material properties for concrete and steel bars at elevated temperatures was not considered in the finite element analysis (FEA) model. The concrete damaged plasticity (CDP) model was used for the concrete material in the test frame. The cube compressive strength of C30 concrete obtained from the cube compressive tests was 30.79 MPa. The parameters of the CDP model are presented in Table 2. The constitutive model for steel bars adopted a bilinear model. The yield and ultimate strengths of the steel bars obtained through the tensile tests were 464.0 and 639.2 MPa, respectively.

Table 1 Reduction coefficients of yield strength and elastic modulus of steel materials at high temperatures

Temperature/℃	20	100	200	300	400	500	600	700	800
Reduction coefficient of yield strength	1.000	0.993	0.947	0.938	0.876	0.642	0.413	0.175	0.096
Reduction coefficient of elastic modulus	1.000	0.983	0.952	0.826	0.701	0.629	0.365	0.102	0.087

Table 2 Parameters of the CDP model

Dilation angle/(°)	Eccentricity	f_{b0}/f_{c0}	K	Viscosity parameter
30	0.1	1.16	0.666 7	5×10^{-4}

3.2 Geometric model and mesh generation

The geometric model was established according to the accurate dimensions of the test frame. It comprised of components, such as concrete slabs, steel columns, steel beams, secondary beams, and ground, as shown in Fig. 15. In the FEA model, the concrete slabs were simulated using the shell element S4R, and the steel bars inside the slabs were set using the Rebar layer method. The steel columns, steel beams, and secondary beams were simulated using the beam element B31. The ground was set as the analytical rigid body. The unstable failures of the steel columns subjected to fire are the main factors causing the progressive collapse of the structure. Therefore, the grid size of the steel columns was relatively dense and set to 50 mm. The grid sizes of the steel beams, secondary beams, and concrete slabs were set to 75 mm. The ground was only used to set the contact surface with the frame, so its grid size was relatively sparse and set to 150 mm. The initial imperfection of all steel columns is considered to be 1/1 000 in the model.

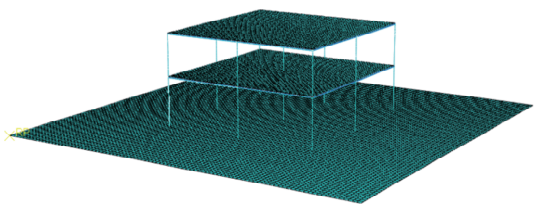

Fig. 15 Geometric model and mesh grid

3.3 Interactions

The M-θ curves of the beam-to-column welded flange-bolted web connection of the test frame under different temperatures can be obtained using the proposed high-temperature component model (see Fig. 16). To accurately reflect the interaction between steel columns and beams in steel frame structures, the connector element is used to simulate the changes in the connection performance of the beam-to-column welded flange-bolted web connection of the test frame under different temperatures, which is represented by the M-θ curves. The connector element is a multi-functional connection element. Compared to the spring element, the connector element has more powerful functions, which can achieve any combination of three translational and three rotational degrees of freedom between two nodes and simulate all common connection forms in engineering practice.

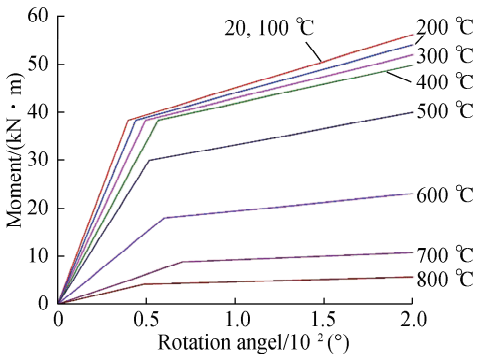

Fig. 16 *M-θ* curves of beam-to-column connection

In the test frame, the stud shear connectors were set between the concrete slab and steel beams. The connection between the concrete slab and steel beams was assumed to be a complete shear connection, i. e., there was no relative slip between the two. In the FEA model, evenly spaced MPC-Beam elements were used to bind the concrete slab and steel beams at all degrees of freedom, as shown in Fig. 17.

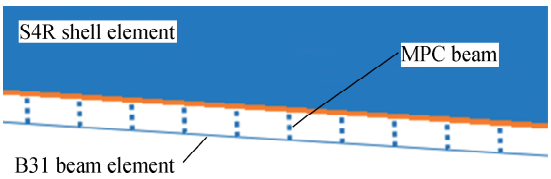

Fig. 17 MPC-beam element

3.4 Boundary conditions and loading method

The steel column base in the test frame is in the form of an exposed rigid joint. Therefore, the bottom ends of all steel columns in the FEA model are simplified as fixed supports. The loading procedure of the FEA model includes the following three aspects, corresponding to the three steps of the model:

1) Gravity load. Take the acceleration due to gravity as $g = 9.8\ \mathrm{m/s^2}$.

2) Floor load. Apply a surface load of $q = 6.0$ kPa perpendicular to the concrete floor.

3) Temperature load. Input the temperature-time curves of all components obtained from the progressive collapse test into the corresponding components in the FEA model through the predefined field method.

4 Numerical Simulation Results

4.1 Failure mode

Fig. 18 shows the failure mode of the test frame obtained from the FEA results. By comparing with Fig. 5, the following observations can be made:

1) In the FEA results, the corner column also suffers the smallest axial constraint. It is the first to experience unstable failure and completely lose its load-bearing capacity, ultimately leading to the progressive collapse of the structure.

2) Regardless of the FEA or test results, no significant bending deformation occurs in the other steel columns, except for the extreme bending deformation of the four fire-exposed steel columns in the test frame. However, large plastic rotational deformation occurs at the end of steel columns.

3) Moreover, the test frame experienced a certain degree of torsion during the progressive collapse process. Thus, the FEA results of the failure mode of the test frame under fire are consistent with the test results.

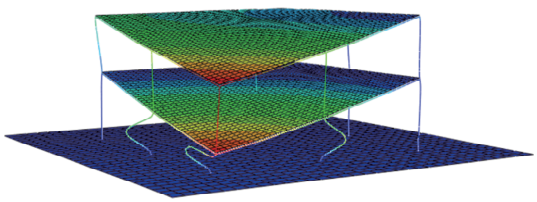

Fig. 18 Failure mode of FEA results

4.2 Displacement-time curves

The displacement-time curves obtained from the FEA results were compared with the test results, as shown in Fig. 19. It can be seen that the displacement-time curves of both results are consistent. The time of progressive collapse of the structure obtained from the FEA results is very close to the test results. The rebalancing points of the structure in the FEA results are obviously lower than those of the test results. This is mainly because the beam and column components are simplified into line elements in the FEA model, leading to a deviation from the actual deformation observed in the tests.

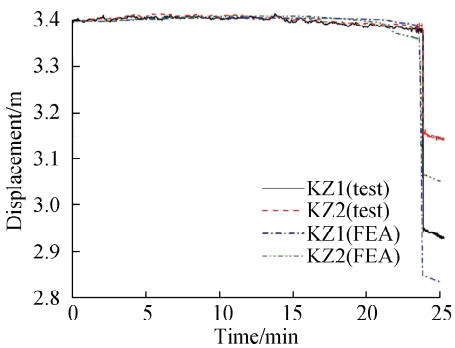

Fig. 19 Comparison of displacement-time curves between FEA and test results

The comparison of failure modes and displacement-time curves between the FEA and test results show that the proposed high-temperature component model of welded flange-bolted web connection can be well applied in the progressive collapse analysis of steel frame structures under fire.

4.3 Axial force-time curves

To further explore the mechanism of the progressive collapse of steel frame structures under fire, the axial force-time curves of the four fire-exposed steel columns (KZ1-KZ4) in the test frame were obtained using the FEA model (see Fig. 20).

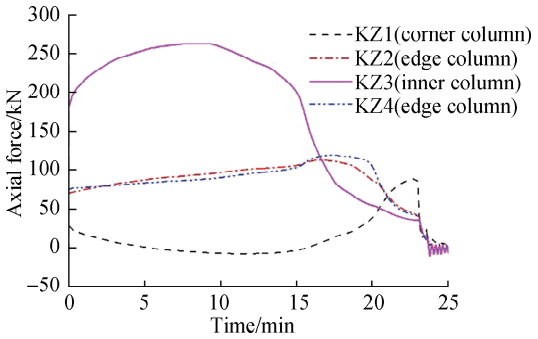

Fig. 20 Axial forces of steel columns subjected to fire

As shown in Fig. 20, the progressive collapse mechanism of the test frame under fire is as follows:

1) The steel columns KZ1-KZ4 expanded under the action of temperature. Due to the maximum axial constraints from the concrete slab and steel beams, the internal force of inner column KZ3 increased most significantly. The bearing capacity of KZ3 continuously declined as the temperature increased. After reaching its ultimate bearing capacity, KZ3 buckled but did not completely withdraw from work, and then its axial force began to decline slowly.

2) The edge columns KZ2 and KZ4 had smaller axial constraints, so their axial forces increased slowly under fire. After reaching their ultimate bearing capacities, KZ2 and KZ4 also buckled without completely withdrawing from work and had a slight decrease in the axial forces.

3) Because the corner column KZ1 was subjected to the weakest constraints, the axial force of KZ1 gradually decreased in the early stage of the fire with the continuous increase in the axial forces of KZ2-KZ4. However, as the axial force of KZ3 decreased, the axial force of KZ1 increased gradually due to the redistribution of internal forces.

4) When the axial forces of KZ2 and KZ4 decreased, the axial force of KZ1 increased rapidly and reached its critical bearing capacity, then KZ1 withdrew from work due to unstable failure.

5) Due to the structural tie action, the other three fire-exposed steel columns also completely lost their bearing capacity almost simultaneously, leading to the progressive collapse failure of the steel frame structure.

5 Conclusions

1) The temperature field of compartment fire is evenly distributed. To simplify the progressive collapse analysis of steel frame structures under fire, the temperature rise curve of all steel columns (or steel beams) under compartment fire is assumed to be the same if their fireproof coating thickness is consistent.

2) The proposed high-temperature component model can accurately predict the behavior and response of welded flange-bolted web connections at high temperatures. The proposed model can also be applied to the progressive collapse analysis of steel frame structures under fire.

3) Under fire within the corner room of a steel frame structure, even though the stress ratio of the corner column is the lowest, the corner column will first lose its load-bearing capacity and withdraw from work because its axial constraint is much smaller than that of the inner and side columns. This triggers the progressive collapse failure of the steel frame structure.

References

[1] Chung H Y, Lee C H, Su W J, et al. Application of fire-resistant steel to beam-to-column moment connections at elevated temperatures[J]. *Journal of Constructional Steel Research*, 2010, **66**(2): 289 − 303. DOI: 10.1016/j.jcsr.2009.09.009.

[2] Shi Y J, Li Z F, Chen H, et al. Experimental research on cyclic behavior of new types of beam column connections in highrise steel frames[J]. *Journal of Building Structures*, 2002, **23**(3): 2 − 7. (in Chinese)

[3] Lew H S, Main J A, Robert S D, et al. Performance of steel moment connections under a column removal scenario. Ⅰ: Experiments[J]. *Journal of Structural Engineering*, 2013, **139**(1): 98 − 107. DOI: 10.1061/(asce)st.1943 − 541x.0000618.

[4] Wang W, Yan P, Li L. Research on joint models of welded flange-bolted web connection for progressive collapse analysis of steel frames[J]. *Engineering Mechanics*, 2014, **31**(12): 119 − 125. (in Chinese)

[5] Ma K. *Seismic fragility analysis of moment-resisting steel frames based on connection failure characteristic*[D]. Nanjing: Southeast University, 2017. (in Chinese)

[6] Wang W Y, Dong Y L. Study of welded flange-bolted web connections of steel structures in fire[J]. *Journal of Hebei Institute of Architectural Science and Technology*, 2006, **23**(2): 24 − 27. (in Chinese)

[7] Mao C J, Chiou Y J, Hsiao P A, et al. Fire response of steel semi-rigid beam-column moment connections[J]. *Journal of Constructional Steel Research*, 2009, **65**(6): 1290 − 1303. DOI: 10.1016/j.jcsr.2008.12.009.

[8] Hu J. *Study on the response of external welded flange-bolted web joints exposed to fire*[D]. Hefei: University of Science and Technology of China, 2009. (in Chinese)

[9] Fan S G, Liang D, Zeng S R, et al. Fire resistance design of the bolted-welded hybrid composite connection in steel frame[J]. *Fire Safety Journal*, 2022, **133**: 103672. DOI: 10.1016/j.firesaf.2022.103672.

[10] Fan S G, Duan S J, Zeng S R, et al. Experimental study and numerical simulation analysis of the Bolted-Welded hybrid connection joint of steel frame under fire[J]. *Structures*, 2022, **41**: 77 − 98. DOI: 10.1016/j.istruc.2022.

04. 100.

[11] Qiang X H, Shu Y, Jiang X, et al. Experimental study on mechanical behavior of high strength steel flange-welded web-bolted connections under fire condition[J]. *Journal of Tongji University* (*Natural Science*), 2022, **50** (10): 1432 − 1442. (in Chinese)

[12] Shi Y J, Shi G, Wang Y Q. A simplified calculation method for moment-rotation curve of semi-rigid end-plate connections[J]. *China Civil Engineering Journal*, 2006, **39**(3): 19 − 23. (in Chinese)

[13] Shi W L, Li G Q. Moment capacity of semi-rigid composite beam-column joints with flush end plate connections: Ⅱ. under positive moment[J]. *China Civil Engineering Journal*, 2007, **40**(9): 30 − 35. (in Chinese)

[14] Wang S F, Chen Y Y. Calculation of initial stiffness of beam-to-column end-plate joint[J]. *Engineering Mechanics*, 2008, **25**(8): 109 − 115. (in Chinese)

[15] Gao J, Shi W L, Li G Q, et al. Initial rotational stiffness of semi-rigid composite beam-to-column joints with flush end plate connections[J]. *Engineering Mechanics*, 2011, **28**(3): 55 − 61.

[16] Heidarpour A, Bradford M A. Behaviour of a T-stub assembly in steel beam-to-column connections at elevated temperatures[J]. *Engineering Structures*, 2008, **30**(10): 2893 − 2899. DOI: 10.1016/j.engstruct.2008.04.007.

[17] Strejček M, Řezníček J, Tan K H, et al. Behaviour of column web component of steel beam-to-column joints at elevated temperatures[J]. *Journal of Constructional Steel Research*, 2011, **67**(12): 1890 − 1899. DOI: 10.1016/j.jcsr.2011.06.004.

[18] Rassati G A, Leon R T, Noè S. Component modeling of partially restrained composite joints under cyclic and dynamic loading[J]. *Journal of Structural Engineering*, 2004, **130**(2): 343 − 351. DOI: 10.1061/(asce)0733-9445(2004)130: 2(343).

[19] Fu Q N. *Dynamic performance study of steel frames based on component-based joint models under progressive collapse*[D]. Chongqing: Chongqing University, 2013. (in Chinese)

[20] Cai X N, Meng S P, Sun W W. Experimental study on performance of components of the exterior self-centering post-tensioned precast connections[J]. *Engineering Mechanics*, 2014, **31**(3): 160 − 167. (in Chinese)

[21] Yuan H. *Analysis of joint stiffness based on component method and improved response surface method*[D]. Guangzhou: South China University of Technology, 2017. (in Chinese)

[22] Yan J. *Study on the semi-rigid beam-column joint under cyclic loading based on component method*[D]. Wuhan: Huazhong University of Science and Technology, 2018. (in Chinese)

[23] Chen X S, Shi G, Zhao J L, et al. Calculation of moment-rotation curves of ultra-large capacity end-plate connections based on component method[J]. *Engineering Mechanics*, 2017, **34**(5): 30 − 41. (in Chinese)

[24] Gao Y Q, Yu H X, Shi G. Research on component-based model for flush endplate connections in fire considering the effect of the shear force[J]. *Building Structure*, 2018, **48**(19): 55 − 60. DOI: 10.19701/j.jzjg.2018.19.012. (in Chinese)

[25] Zhang Y F, Chen Y Y. Component method models for the analysis of end-plate joints with continuous beam and column under cyclic loads[J]. *Progress in Steel Building Structures*, 2018, **20**(4): 47 − 57, 96. DOI: 10.13969/j.cnki.cn31-1893.2018.04.006. (in Chinese)

[26] Tan Z, Zhong W H, Li C F. Research on component joint models of semi-rigid joint model with top and seat angles and double web angles under progressive collapse[J]. *Journal of Disaster Prevention and Mitigation Engineering*, 2019, **39**(3): 445 − 453. DOI: 10.13409/j.cnki.jdpme.2019.03.010. (in Chinese)

[27] Usmani A S, Chung Y C, Torero J L. How did the WTC towers collapse: A new theory[J]. *Fire Safety Journal*, 2003, **38**(6): 501 − 533. DOI: 10.1016/S0379-7112(03)00069-9.

[28] Flint G, Usmani A, Lamont S, et al. Structural response of tall buildings to multiple floor fires[J]. *Journal of Structural Engineering*, 2007, **133**(12): 1719 − 1732. DOI: 10.1061/(asce)0733-9445(2007)133: 12(1719).

[29] Lange D, Röben C, Usmani A. Tall building collapse mechanisms initiated by fire: Mechanisms and design methodology[J]. *Engineering Structures*, 2012, **36**: 90 − 103. DOI: 10.1016/j.engstruct.2011.10.003.

[30] Sun RR, Huang Z H, Burgess I W. Progressive collapse analysis of steel structures under fire conditions[J]. *Engineering Structures*, 2012, **34**: 400 − 413. DOI: 10.1016/j.engstruct.2011.10.009.

[31] Jiang J A, Li G Q, Usmani A. Progressive collapse mechanisms of steel frames exposed to fire[J]. *Advances in Structural Engineering*, 2014, **17**(3): 381 − 398. DOI: 10.1260/1369-4332.17.3.381.

[32] Agarwal A, Varma A H. Fire induced progressive collapse of steel building structures: The role of interior gravity columns[J]. *Engineering Structures*, 2014, **58**: 129 − 140. DOI: 10.1016/j.engstruct.2013.09.020.

[33] Qin C, Mahmoud H. Collapse performance of composite steel frames under fire[J]. *Engineering Structures*, 2019, **183**: 662 − 676. DOI: 10.1016/j.engstruct.2019.01.032.

[34] Chen S C, Tian X K, Zhang L, et al. Experimental study on the initial collapse mechanism of multi-story steel frames under localized fire[J]. *Journal of Disaster Prevention and Mitigation Engineering*, 2015, **35**(1): 113 − 118. DOI: 10.13409/j.cnki.jdpme.2015.01.019. (in Chinese)

[35] Jiang B H, Li G Q, Li L L, et al. Simulations on progressive collapse resistance of steel moment frames under localized fire[J]. *Journal of Constructional Steel Research*, 2017, **138**: 380 − 388. DOI: 10.1016/j.jcsr.2017.05.018.

[36] European Committee for Standardization. Design of steel structures, Part 1 − 8: Design of joints: Eurocode 3, EN 1993-1-8[S]. Belgium: European Committee for Standardization, 2005.

[37] Yim H C, Krauthammer T. Mathematical-mechanical model of WUF-B connection under monotonic load[J]. *Engineering Journal*, 2010, **47**(2): 71 − 90.

[38] ABAQUS. *ABAQUS user's manual, version* 2022[M]. Pawtucket, RI, USA: Hibbitt, Karlsson & Sorensen,

Inc., 2022.
[39] European Committee for Standardization. Design of steel structures, Part 1-2: General rules—Structural fire design: Eurocode 3, EN 1993-1-2[S]. Belgium: European Committee for Standardization, 2005.

基于高温组件模型的火灾下钢框架结构连续倒塌分析

丁润民　范圣刚

（东南大学混凝土及预应力混凝土结构教育部重点实验室，南京 211189）
（东南大学土木工程学院，南京 211189）

摘要：为探究火灾下钢框架结构的整体行为反应和连续倒塌机制，对一个 1∶2 缩尺钢框架结构开展了角部房间受火工况下的连续倒塌试验，获得了火灾发展全过程的空气温度-时间曲线、构件温度-时间曲线和框架位移-时间曲线，以及火灾下钢框架结构的连续倒塌破坏模式. 基于组件法构建了栓焊节点的高温组件模型，推导了高温下栓焊节点弯矩-转角曲线的双折线数学模型. 在此基础上，建立了包含栓焊节点高温组件模型的火灾下钢框架结构连续倒塌有限元分析模型，通过与连续倒塌试验结果进行对比，验证了有限元分析模型的准确性，并揭示了火灾下钢框架结构的连续倒塌机制. 研究结果表明，钢框架结构在角部房间受火工况下，角柱虽然应力比最低，但由于受到的轴向约束远小于内柱和边柱，将率先丧失承载能力，并退出工作，引发钢框架结构连续倒塌破坏.

关键词：火灾；组件模型；栓焊节点；连续倒塌；钢框架
中图分类号：TU391